Marangoni convection using computational fluid dynamics via a continuum surface force

Bruce E. Ciccotosto and Caleb S. Brooks†

Department of Nuclear, Plasma & Radiological Engineering, University of Illinois, Urbana-Champaign, IL 61801, USA

(Received xx; revised xx; accepted xx)

A two-dimensional box with two fluids undergoing Marangoni convection is simulated using computational fluid dynamics and results are compared with previous analytical, numerical, and experimental results. Previous results are used as validation benchmarks for the development of a variable surface tension model within openFOAM. The steady state orientation of the two fluid interface is found to change in sign and magnitude depending on the conditions.

more on conclusions

Key words: two phase flow, Marangoni, surface tension, heat pipes, CFD

1. Introduction

Viscosity in a fluid is a macroscopic property due to the isotropic interactions of particles in the bulk fluid. Surface tension arises from the imbalance of these interactions normal to the interface between phases. Local changes in temperature or species concentration will create gradients in these interactions, resulting in an imbalance tangential to the interface. The tangential imbalances create what is called Marangoni convection, and fluid will move from areas of lower surface tension to areas of higher surface tension. The areas of low surface tension "hold together" less strongly and thus the fluid "expands" towards areas of higher surface tension, whereas the areas of higher surface tension "pull in" fluid from elsewhere. In most fluids, the change in the surface tension coefficient with temperature, γ, is nearly linear and negative. As a result, a local increase in temperature gives a linear decrease in the local normal surface tension coefficient, σ. Surface tension and Marangoni convection can be exploited in small scale heat transfer devices such as heat pipes. These devices are used ubiquitously across many industries (Srimuang & Amatachaya 2012).

A heat pipe schematic without a wick (sometimes called a thermosyphon) is shown in figure 1. The liquid phase clings to the ends and sides, while a vapour core exists in the centre. For maximum heat transfer, vapour convection should be toward the cold end, and liquid convection away from the cold end. Evaporation occurs at the hot end, and the pressure of the vapour increases, the resulting pressure gradient moves vapour towards the cold end. Condensation then occurs at the cold end and liquid forms, causing wicking away from the cold end. If $\gamma < 0$, Marangoni convection causes liquid convection towards the cold end, opposing the wicking action. This reduces the overall performance and can cause the liquid to detach from the wall in some cases (Nguyen *et al.* 2020). If $\gamma > 0$,

† Email address for correspondence: csbrooks@illinois.edu

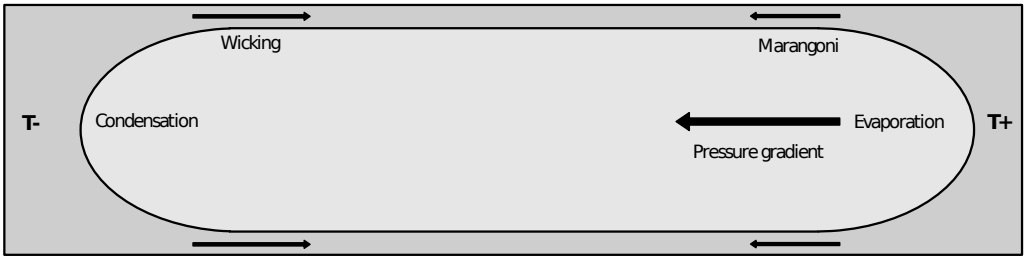

FIGURE 1. Heat Pipe Schematic and Convection Mechanisms

Marangoni forces would aid performance and liquid convection acts away from the cold end. Given the importance of surface tension in the physics of heat pipes, it is critical for modelling to capture the dependence of temperature and predict the resulting flow.

An idealized benchmark for modelling these physics is a simple two phase flow in a box, demonstrated by figure 2. The two-dimensional box contains liquid to a height h and is placed under a temperature gradient between the two side walls. A deformed interface from Marangoni convection is shown by the dashed line. This benchmark has been used in several previous analyses.

Sen & Davis (1982) found an analytical solution for the single-phase stream function by asymptotic analysis. Their analysis also captures the interface deformation and provides an expression based on the capillary number. The model assumes an incompressible steady-state single phase flow with an aspect ratio h/L approaching zero. The effects of buoyancy are not considered.

Villers & Platten (1992) experimented with Marangoni convection of acetone and studied velocity profiles and instabilities of the rolling vortices observed. They took multiple velocity profile measurements at $x = L/2$ and compared to a single-phase CFD model. Their model applied the Marangoni forces at a fixed interface above the liquid. The same authors also developed an analytical model to approximate the velocity profile for an arbitrary value of γ (Villers & Platten 1987). Their model reduces to that from Sen & Davis (1982) for moderate negative values of γ. The original authors note that the magnitude of the velocity is not well captured but qualitatively agrees with the shape from their experimental results.

Zhou & Huang (2010) studied a two-fluid incompressible system without buoyancy and with largely varying Prandtl numbers between fluids. They found that the interface deformation was reversed to that predicted by Sen & Davis (1982). The sensitivity of this reversal phenomenon is unknown, as Zhou & Huang (2010) studied a single Pr ratio of nearly 9300:1. In heat pipes the two fluids are both nearly at saturation, meaning the difference in Pr will be small under vapour super heating, $\sim O(2)$.

Chen & Xu (2021) found various transient regimes in this problem by analysing the velocity and time scales of Marangoni convection and viscous effects. Their analysis and CFD model, compared against results from Villers & Platten (1992); Sen & Davis (1982), also neglects interface deformation and the surface tension forces are applied at a fixed interface.

The commercial CFD code STAR-CCM+ models Marangoni convection by the continuum surface force (CSF) based on the work from Brackbill *et al.* (1992), but is closed source. Ongoing work by Scheufler & Roenby (2021) seeks to expand the openFOAM family of solvers and has released a framework that includes a model for temperature varying normal surface tension, but does not consider any tangential forces. The objective of the present work is to; investigate the impact of a variety of factors on the velocity

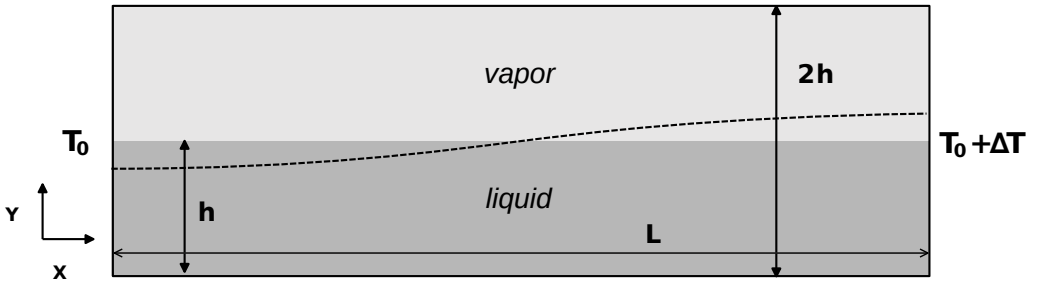

FIGURE 2. Domain and Boundary Conditions

and interface profiles of the idealized Marangoni benchmark; develop and validate a CFD model for Marangoni convection on a free surface using openFOAM. This is accomplished by revisiting the factors influencing interface deformation in Marangoni convection and the development of a variable surface tension model using volume of fluid (VOF) method. The resulting model is implemented in the open source CFD project openFOAM and validated against previous results as well as predictions from STAR-CCM+. Factors considered include; force of gravity, a range of Marangoni numbers, vapour compressibility, liquid equation of state, and different boundary conditions.

2. Problem Setup

2.1. *Boundary and Initial Conditions*

The flow domain is a two-dimensional box of dimensions $2h$ by L as illustrated in figure 2. The top and bottom walls are insulated, while the left and right are constant temperature. All walls enforce the no slip velocity condition. The liquid phase is initially at a uniform height h, such that for $y < h, \alpha = 1$ and zero otherwise. The initial temperature field is a linear fit between the two temperature boundaries. If present, gravity acts in the negative y direction. When the domain is referred to as "open" this means a symmetry plane was used on the top boundary. This allows a velocity component normal to the boundary and acts as a von Neumann boundary for all other variables. This was chosen to more closely match the analysis from Sen & Davis (1982) who considered a two-dimensional slot without a top wall and neglected effects of the vapour (i.e. single phase).

In this domain, with $\gamma < 0$, fluid at the interface will convect in the negative x direction. The return flow at the cold wall will then create a counterclockwise vortex cell. The mass flux of these two phenomena (Marangoni convection and the return flow) are equal in steady state, but their velocities of are not equal. Marangoni convection occurs only at the very thin interface (moving the fluid left), while the return flow occurs throughout the rest of the liquid depth (moving fluid to the right). The profile of the interface will then deform, as the balance between Marangoni convection and the return flow may not balance with a flat interface. At large Ma, the vortex cells may detach, and multiple cells may appear (Villers & Platten 1992; Smith & Davis 1983).

2.2. *Governing Equations*

The relevant physics to capture in this type of flow problem are then normal surface tension, tangential surface tension, compressibility, buoyancy, viscous forces, and phase interactions. The effects of phase change are not considered in the current model to simplify the validation of Marangoni convection. As such, there are no source terms in

the governing equations, surface tension is accounted for in the body force term of the momentum and energy equations. In the present work, the transient form of the governing equations is solved until reaching steady state for added numerical stability.

Formulation of the problem can begin from the general conservation equation in differential form based on the continuum assumption,

$$\frac{\partial \rho\psi}{\partial t} + \nabla \cdot (\boldsymbol{v}\rho\psi) + \nabla \cdot \boldsymbol{J} = \rho\phi. \tag{2.1}$$

Where ψ is a scalar field, $\boldsymbol{J}$ is a flux through the control volume, and ϕ is a volume potential. For most of the governing equations $\boldsymbol{J}$ and ϕ will be zero as there will be no source terms in the bulk or fluxes at the domain boundaries. By letting $\psi = 1, \boldsymbol{J} = 0$, and $\phi = 0$, and expanding the divergence term, the continuity equation is,

$$\frac{D\rho}{Dt} + \rho\nabla \cdot \boldsymbol{v} = 0. \tag{2.2}$$

In general, the compressible form above is used, but for the specified incompressible cases $\nabla \cdot \boldsymbol{v} = 0$ is solved. The conservation of momentum is found by letting $\psi = \boldsymbol{v}, \boldsymbol{J} = P\boldsymbol{I} - \boldsymbol{T}$, and $\phi = \boldsymbol{f}_b$, and given as,

$$\frac{\partial \rho\boldsymbol{v}}{\partial t} + \nabla \cdot (\rho\boldsymbol{v}\boldsymbol{v}) = \nabla \cdot \boldsymbol{T} - \nabla P + \rho\boldsymbol{f}_b, \tag{2.3}$$

where the vector $\boldsymbol{f}_b$ is a volumetric body force, $\boldsymbol{I}$ is the identity tensor, and $\boldsymbol{T}$ is the viscous stress tensor for a Newtonian fluid. Expanding the divergence time derivative terms on the left-hand side of (2.3) gives,

$$\rho\frac{D\boldsymbol{v}}{Dt} + \boldsymbol{v}\left(\frac{\partial \rho}{\partial t} + \nabla \cdot \rho\boldsymbol{v}\right) = \nabla \cdot \boldsymbol{T} - \nabla P + \rho\boldsymbol{f}_b. \tag{2.4}$$

This can be simplified by noting that (2.2) is present in the second term which must be zero. The final form of the momentum equation is then,

$$\frac{D\boldsymbol{v}}{Dt} = \frac{1}{\rho}\nabla \cdot \boldsymbol{T} - \frac{\nabla P}{\rho} + \boldsymbol{f}_b \tag{2.5}$$

For the conservation of energy, the total enthalpy form is used from: $\psi = h - \frac{P}{\rho}, \boldsymbol{J} = q - P\boldsymbol{I}$, and $\phi = 0$. Here h is the total enthalpy, q is the heat flux at the control volume surface, and the effects of viscous heating are neglected. Substituting into (2.1), expanding the divergence terms on the left-hand side, replacing q with Fourier's law, and collecting pressure terms gives,

$$\rho\frac{Dh}{Dt} + h\left(\frac{D\rho}{Dt} + \rho\nabla \cdot \boldsymbol{v}\right) = k\nabla^2 T + P\nabla \cdot \boldsymbol{v} + \boldsymbol{v} \cdot \nabla P + \frac{\partial P}{\partial t} + \rho\boldsymbol{f_b} \cdot \boldsymbol{v}. \tag{2.6}$$

On the left-hand side is the total enthalpy h multiplied with the mass continuity from (2.2), which must be zero. With some rearranging of the pressure terms the final form of the enthalpy conservation is,

$$\rho\frac{Dh}{Dt} = k\nabla^2 T + \frac{DP}{Dt} + P\nabla \cdot \boldsymbol{v} + \rho\boldsymbol{f_b} \cdot \boldsymbol{v}. \tag{2.7}$$

The volume fraction continuity is found by letting $\psi = \alpha, \boldsymbol{J} = 0$, and $\phi = 0$,

$$\frac{\partial \rho\alpha}{\partial t} + \nabla \cdot (\boldsymbol{v}\rho\alpha) = 0, \tag{2.8}$$

where α is the volume fraction of the primary phase. Again expanding the divergence

term, and dropping the mass continuity from (2.2) leaves the material derivative of the volume fraction,

$$\frac{D\alpha}{Dt} = 0. \tag{2.9}$$

2.3. *Surface Tension Model*

Marangoni convection is implemented in openFOAM as a continuum surface force based on the work from Brackbill *et al.* (1992). STAR-CCM+ reports using the same formulation but is closed source. The normal component of the surface tension force is given from the familiar,

$$\boldsymbol{f}_{\sigma,n} = \sigma\kappa\hat{\boldsymbol{n}}. \tag{2.10}$$

Where the surface tension coefficient now becomes a linear function of temperature,

$$\sigma = \gamma T - \gamma\left(T_0 + \frac{\Delta T}{2}\right) + \sigma_0, \tag{2.11}$$

giving the nominal σ_0 at the centre of the box when $T = T_0 + \Delta T/2$. The surface unit normal vector $\hat{\boldsymbol{n}}$ is found from the gradient of the volume fraction field,

$$\hat{\boldsymbol{n}} = \frac{\nabla\alpha_i}{|\nabla\alpha_i|}. \tag{2.12}$$

The surface curvature, κ, is found from the divergence of the unit normal

$$\kappa = -\nabla\cdot\hat{\boldsymbol{n}} = -\nabla\cdot\left(\frac{\nabla\alpha_i}{|\nabla\alpha_i|}\right). \tag{2.13}$$

Marangoni convection occurs to due to variations in σ, which results in a force that acts *along* the interface. Therefore, the tangential variation of the temperature field along the interface is needed. This can be found from,

$$\nabla_t T = \nabla T - \hat{\boldsymbol{n}}(\hat{\boldsymbol{n}}\cdot\nabla T). \tag{2.14}$$

The subscript t denotes the surface tangent direction. The first term is the gradient of temperature and the second term is the variation in the normal direction. The subtraction of the normal direction from the full gradient gives just the tangential variation. Multiplying by the derivative of the surface tension coefficient with respect to temperature, γ, gives the tangential force component,

$$\boldsymbol{f}_{\sigma,t} = \gamma(\nabla T - \hat{\boldsymbol{n}}(\hat{\boldsymbol{n}}\cdot\nabla T). \tag{2.15}$$

The total surface tension force is then the sum of (2.15) and (2.10) and applied per volume,

$$\boldsymbol{f}_{\sigma} = |\nabla\alpha_i|\left(\gamma(\nabla T - \hat{\boldsymbol{n}}(\hat{\boldsymbol{n}}\cdot\nabla T) + \sigma(T)\kappa\hat{\boldsymbol{n}}\right). \tag{2.16}$$

The leading factor of $|\nabla\alpha_i|$ effectively filters the equation to only cells near the interface. (i.e. the gradient of the volume fraction is zero away from the interface.) This can be simplified by noting the definition of $\hat{\boldsymbol{n}}$,

$$\boldsymbol{f}_{\sigma} = |\nabla\alpha_i|\left(\gamma(\nabla T - \hat{\boldsymbol{n}}(\hat{\boldsymbol{n}}\cdot\nabla T)\right) + \sigma(T)\kappa\boldsymbol{n}. \tag{2.17}$$

2.4. *Definition of the Flow Problem*

To fully define problem, the following nondimensional numbers are needed: Rayleigh number Ra, Prandtl number Pr, Marangoni number Ma, and Capillary number Ca. Chen & Xu (2021) and Sen & Davis (1982) did not include the Rayleigh number in their

k	ρ_0	ΔT	T_0	β	σ_0	P_0	h	L	$\mathbf{g}$
0.1	1	1	299	1/300	0.01	101325	1/12	1	0, 9.81

TABLE 1. Reference Values

analyses as they neglected buoyancy effects, and the experimental work by Villers & Platten (1992) did not control for the Capillary number.

Some previous authors defined the aspect ratio inversely or did not include it. For consistency the set of nondimensional numbers will be defined with an aspect ratio h/L and use a characteristic length of h. The Prandtl number is defined in the usual way,

$$Pr = \frac{\nu}{\alpha}, \tag{2.18}$$

while the capillary number will be defined as,

$$Ca = \frac{|\gamma|\Delta T h}{\sigma_0 L}. \tag{2.19}$$

In this form it expresses the ratio of tangential surface tension to the normal component, scaled by the aspect ratio. The Rayleigh number is given by

$$Ra = \frac{g\beta\Delta T h^4}{\alpha\nu L}, \tag{2.20}$$

where the expansion coefficient, β, is approximated as $(T_0 + \Delta T)^{-1}$. The Marangoni number is given by,

$$Ma = \frac{|\gamma|\Delta T h^2}{\alpha\mu L}. \tag{2.21}$$

While the Reynolds number is found by the relation,

$$Re = \frac{Ma}{Pr} = \frac{\rho_0|\gamma|\Delta T h^2}{\mu^2 L}, \tag{2.22}$$

but is not required to constrain the problem if (2.18 - 2.21) are held constant.

For a case of interest, the nondimensional numbers are chosen, along with reference values of $k, \rho_0, \Delta T, T_0,\ g, L, h,$ and a reference pressure P_0. The remaining variables, α, ν, μ, γ and σ_0, are found by the previous definitions. From substituting (2.18) into (2.20) the thermal diffusivity is found by,

$$\alpha = \sqrt{\frac{g\beta\Delta T h^4}{RaPrL}}. \tag{2.23}$$

The kinematic and dynamic viscosities are then found via the Prandtl number. The change in surface tension coefficient is then obtained from (2.21),

$$|\gamma| = \frac{\alpha\mu L}{Ma\Delta T h^2}, \tag{2.24}$$

and taken as negative. The reference normal surface tension coefficient is then found by,

$$\sigma_0 = \frac{|\gamma|\Delta T h}{CaL}. \tag{2.25}$$

The chosen constant parameters are listed in table 1 in SI units. If there is no gravity, the Rayleigh number becomes zero and the material properties are then taken from the

corresponding 1g case. For most cases, the liquid density is taken as a constant ρ_0. A few cases linearly varied the liquid density with temperature as,

$$\rho = \rho_0 - \rho_0\beta(T - T_0). \tag{2.26}$$

The surface tension coefficient is obtained from (2.11), and all other material properties are held constant. Even though the underlying mechanics that cause viscosity and surface tension are the same, the viscosity is held constant in the present work. In these idealized box flow cases, the temperature gradients are quite moderate and changes in the inertial terms of the governing equations from variation of viscosity would be small.

3. Analytical Model

An analytical solution for the stream function of this problem in the limit of small aspect ratio was found by Sen & Davis (1982). Their solution for the interface height, given below in (3.1), will be used to compare some numerical results. Here it is presented in terms of physical parameters as,

$$h_*(x_*) = 1 + \frac{\gamma\Delta T}{\sigma_0 h 16}\left[(2x_* - 1)^3 - 3(2x_* - 1)\right]. \tag{3.1}$$

This can be made dimensional by scaling with the nominal interface height prior to Marangoni convection. Sen & Davis (1982) give a confidence range for (3.1) of $\pm(h/L)^2$. The solutions from Sen & Davis (1982) have been used multiple times to model the velocity profile of liquid under Marangoni convection with the below quadratic form,

$$U_*(y) \sim \frac{3}{4}y_*^2 - \frac{1}{2}y_*, \tag{3.2}$$

which shows the overall shape of the profile but not its magnitude. Some previous work simply takes fits a quadratic profile to their results to show agreement with Sen & Davis (1982). This is insufficient and unnecessary because the magnitude of the velocity profile can be recovered by using the original stream function from Sen & Davis (1982).

Starting from equation 5.3a from Sen & Davis (1982), and substituting their parameter definitions, the stream function in terms of physical parameters is,

$$\psi(x_*, y_*) = \frac{1}{4}y_*^2(y_* - 1) + \frac{h^2|\gamma|\Delta T}{64L^2\sigma_0}y_*^3\left[4x_*^2 - 3x_* + \frac{4}{3}m(12x_*^2 - 1)\right]. \tag{3.3}$$

The variable m is taken as zero corresponding to a 90° contact angle with the side walls. The second term contains Ca, based on (2.19) which is typically $O(10^{-3})$ or less. Therefore, the second term can be neglected as it is small compared to the first. Taking the partial derivative with respect to y_* yields a function for the nondimensional velocity in the x_* direction,

$$\frac{\partial\psi}{\partial y} = \frac{3y_*^2}{4} - \frac{y_*}{2}. \tag{3.4}$$

The characteristic velocity of the flow will be defined as,

$$U_c \equiv \frac{|\gamma|\Delta T h}{\mu L} = \frac{Ma}{Pr}\frac{\nu}{h}. \tag{3.5}$$

This velocity scale gives a sense of how dominant Marangoni forces are over the viscous forces, and again considers the aspect ratio. Equation 3.4 is then scaled with the

dimensional U_c and a leading coefficient,

$$U_{xm} = CU_c \left(\frac{3y_*^2}{4} - \frac{y_*}{2} \right), \tag{3.6}$$

which is the dimensional velocity in the x direction as a function of position y_* with a yet undetermined coefficient, C. To nondimensionalize (3.6), the dimensional velocity is defined equivalently as,

$$U_x \equiv U_* U_c \frac{h}{L}, \tag{3.7}$$

where the aspect ratio h/L is considered. This gives the nondimensional form as,

$$U_* = \frac{U_x}{U_c} \frac{L}{h}. \tag{3.8}$$

Substituting the dimensional velocity from the model (3.6), into (3.8) gives,

$$U_{*m} = \frac{U_{xm}}{U_c} \frac{L}{h} = \left(\frac{3y_*^2}{4} - \frac{y_*}{2} \right) \frac{L}{h} C. \tag{3.9}$$

This expression comes with all the limitations and assumptions of the original expressions from Sen & Davis (1982).

A more generalized velocity profile for any value of γ uses a cubic profile (Villers & Platten 1987). An expression similar to (3.9) can be also be obtained. However, the recovery of the magnitude would require some additional work as it is not independent of Ma in the cases studied here. In the present work, only (3.9) based on the work from Sen & Davis (1982) will be compared to the results.

4. CFD

In both CFD models, the PISO and SIMPLE methods are used for solving the governing equations with the chosen physics of each scenario. Initial conditions and boundary conditions are described in §2.1. Relaxation factors and solver settings were left as default in both models. Contact angles on all boundaries were set at 90 deg.

4.1. *STAR-CCM+ Setup*

STAR-CCM+ provides an intuitive menu selection for the desired physics that adapts the options available based on the previous selection. Models were generally chosen to replicate as close as possible the models in openFOAM. In the present work, the VOF model was selected which requires the 'multiphase model' and the segregated solver. The Space model was two-dimensional, all cases were laminar, and the gravity model was also selected. For energy conservation, the 'Segregated Multiphase Temperature' is used, which according to the documentation, "solves the total energy equation with temperature as the solved variable. Enthalpy is then computed from temperature according to the equation of state." There are currently no other energy equation solution methods available for this physics configuration in STAR-CCM+. Within phase interations, the surface tension model was selected with Marangoni convection enabled. The semi-implicit formulation was not selected.

4.2. *openFOAM Implementation*

The tangential surface tension force, (2.15), was implemented in openFOAM v2106. There are a variety of multiphase solvers available in this release and the compressible-MultiphaseInterFoam solver was chosen as the starting point for development in the

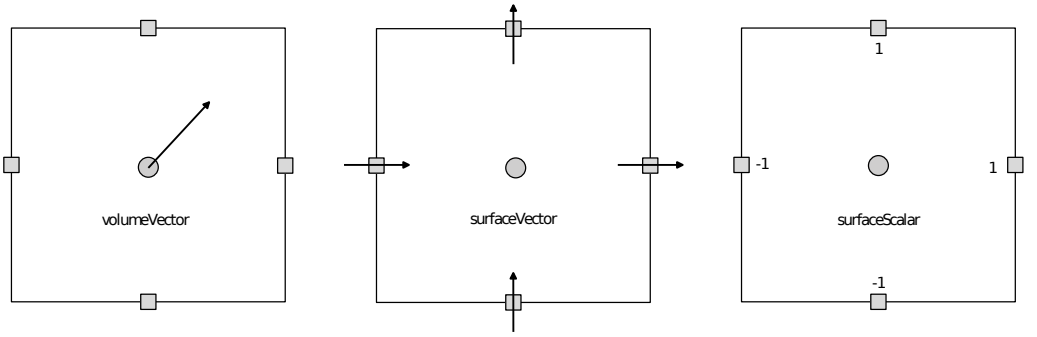

FIGURE 3. Schematic showing equivalence of openFOAM fields: ∘ denotes the cell centred nodes, □ denotes the face centre nodes.

present work. This is an N-phase compressible solver that includes effects models for constant normal surface tension, and wall contact angle. The Marangoni model presented here is currently limited to two phases, however. This solver uses the thermophysical properties library and many combinations of models are possible. The internal energy form of energy conservation is solved. Each phase uses the heRhoThermo type which is then reconstructed into the mixture properties by the solver at runtime.

4.2.1. *VOF and Finite Volume*

Using VOF method introduces an additional caveat for interface calculations. The interface normal vectors for *both* phases must be considered as all phases share a pressure field and only one continuity equation is solved. Equation (2.15) is still valid in its current form, however $\hat{\boldsymbol{n}}$ is slightly different and contains the volume fraction gradients (the interface normals) of both phases. This is demonstrated by algorithm 1 in line 2.

The solver uses the finite volume method (FVM), meaning quantities are solved at the face centred nodes rather than the cell centred nodes as in finite difference methods. These face centred nodes are sometimes referred to as the "half" grid-points. Special care must be taken to ensure distinction from cell centred values (referred to in openFOAM parlance as volume fields) and face centred values (surface fields). Any scalar or vector quantities can be converted freely between the volume and surface data types. For example, a volume-scalar can be converted to a surface-scalar via interpolation from mesh centroids to cell faces. A volume-vector can be projected from the mesh centroids onto the cell faces, giving a flux at the cell face, resulting in a surface-scalar.

To show the equivalence graphically, consider figure 3, here a volume-vector is placed at the cell centre. This vector can be equivalently represented as vectors at each of the cell faces (surface-vector), or as a scalar flux at each cell face (surface-scalar).

Algorithm 1 Calculate Surface Tension Force

1: **while** calculate.STF **do**
2: n12 = $\alpha_2\nabla\alpha_1 - \alpha_1\nabla\alpha_2$; ▷ normal of phases 1 and 2, volVectorField
3: nHat = n12 / mag(n12); ▷ Eqn. 2.12, volVectorField
4: tangentVector = $\gamma(\nabla T - (\text{nHat}\cdot\nabla T)\cdot\text{nHat}$; ▷ Eqn. 2.15, volVectorField
5: tangent = tangentVector · meshFaceNormals; ▷ project to surfaceScalarField
6: calculate σ ▷ Eqn. 2.11
7: normal = σ interp(κ) n12 · meshFaceNormals; ▷ Eqn. 2.10, surfaceScalarField
8: STF += interp(mag(n12))tangent + normal; ▷ Eqn. 2.17, surfaceScalarField
9: **end while**

Scenario	Gravity	Liquid Density	Vapour Density	Domain	Orientation	Max Height
S1	0g	ρ_0	ideal	closed	+	1.001
S2	0g	ρ_0	ideal	open	−	1.051
S3	1g	ρ_0	ideal	closed	+	1.002
S4	1g	ρ_0	ideal	open	−	1.001
S5	-	ρ_0	ρ_0	closed	0	1
S6	-	ρ_0	ρ_0	open	−	1.053
S1B	0g	eq. (2.26)	ideal	closed	+	∼1
S3B	1g	eq. (2.26)	ideal	closed	+	1.0036

TABLE 2. Summary of Conditions and Final Interface Orientation

After constructing the tangential surface tension force from (2.15), the volume-vector is then converted to a surface-scalar by taking the inner product with the cell face normals. This is shown in algorithm 1 on line 5. For more details on the implementation, see the full source code on GitHub [citation of my repository].

5. Results

The steady state timescale for the numerical solution is estimated based on a fluid parcel moving at the characteristic velocity from (3.5) over the domain length L around five times. For the cases considered, this gives a physical time of around $15 - 25$ sec. For most cases, a time-step of 10^{-3} sec was used. This equates to around 5 minutes of wall time per case. All results presented used a 600×100 isotropic hexahedral grid for the $2h \times L$ domain. While some results are presented as nondimensional (or scaled dimensionally when relevant for comparison), the CFD models solve the dimensional form of the governing equations, and a domain size of $2/12 \times 1$ m was used, giving a grid sizing ~ 1.66mm. Previous work found grid independence on this flow problem with coarser grids (Chen & Xu 2021). Regardless of the numerical scheme or mesh resolution, interface diffusion was found near the cold wall at $x^* = 0$, shown in figure 4. While this is concerning, mass was still conserved to a high degree in every case ($< 10^{-8}$ kg lost). The most likely explanation is the compressible formulation used in the VOF method, as incompressible scenarios have this issue to a less degree as seen from S5 and S6 in figure 5. The focus of this work is the implementation and validation of the physics, and not to get caught up in numerics and CFD specific issues that arise. As such, the spatial and temporal discretization was deemed more than sufficient for this goal. If future work implementing evaporation models finds the interface diffusion from VOF to be problematic, then other multiphase methods such as isoAdvector or level-set methods will be tested.

5.1. *Effect of Marangoni number*

In table 2, the cases investigated are summarized, the interface is taken at $\alpha = 0.5$. The interface height for S3 over a range of Ma is shown in figure 4, and there is excellent agreement between the STAR-CCM+ and openFOAM results.

Figure 4 shows the velocity profiles from S3 with varying Ma, along with the prediction from (3.9). Again good agreement is seen between STAR-CCM+ and openFOAM RMS?. The magnitude of the velocity doesn't vary much with changes in Ma and can conclude the velocity profile is independent of the Marangoni number for S3. Only the openFOAM case with $Ma = 1267$ deviates. This may be due to a difference in numerical

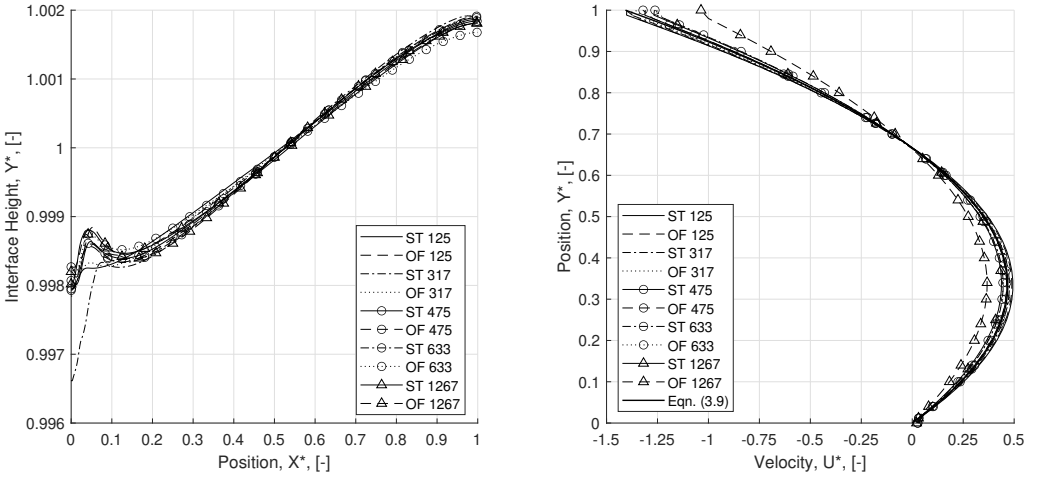

FIGURE 4. Effect of Marangoni number on interface position in S3 (left) and velocity profile in S3 (right), predictions from STAR-CCM+ (ST) and openFOAM (OF)

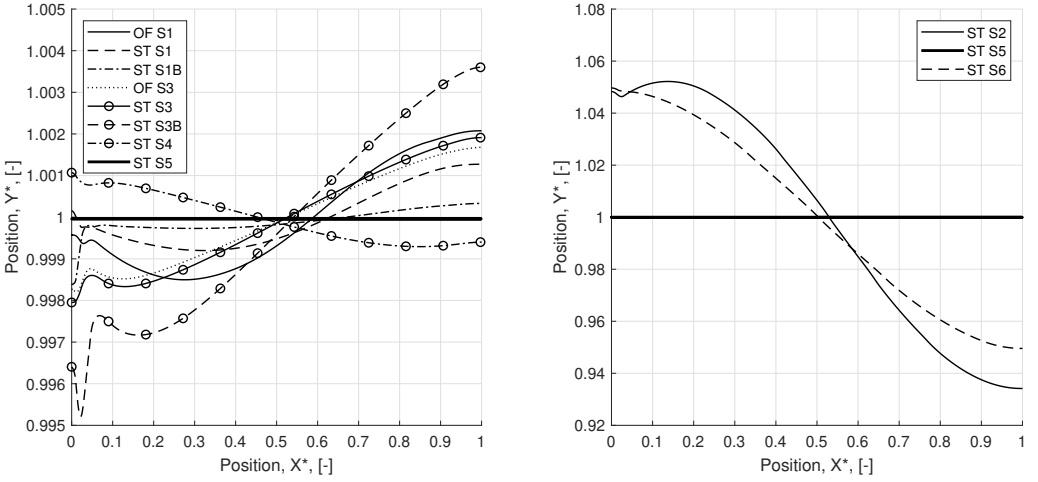

FIGURE 5. Interface height in different scenarios, constant Ma number 633, predictions from STAR-CCM+ (ST) and openFOAM (OF)

implementation between STAR-CCM= and openFOAM that only becomes apparent at higher Marangoni number. Future work should investigate a wider range, on the order of 10-100× larger.

5.2. *Effect of Scenario*

In figure 5, the interface shape is plotted for all scenarios. If the CFD models were perfect, each line would be symmetric about $x_* = \frac{1}{2}$ and intersect the line $y* = 1$. This again shows the smearing limitations of the VOF method. When the domain is open, the interface slope becomes negative, as shown in S2, S4, and S6. If there are no gravitational effects, the maximum height of the interface becomes much larger, as shown by S2 and S6. If the domain is closed, the interface slope becomes positive (S1, S3, S5, S1B, and S3B), and gravity does not have much effect the magnitude, unless both phases are constant density where the interface remains level as in S5.

The results in figure 6 show that $C \sim 0.468$ and holds constant independent of the

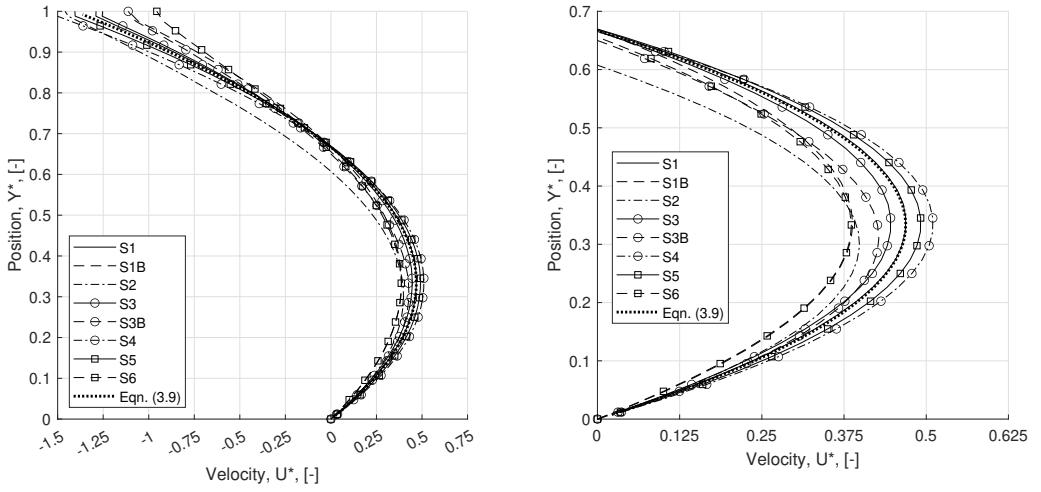

FIGURE 6. Velocity profile at $x^* = L/2$ in different scenarios, constant Marangoni number 633, predictions from STAR-CCM+ (ST) and eqn. (3.9). Full profile (left) and zoomed (right).

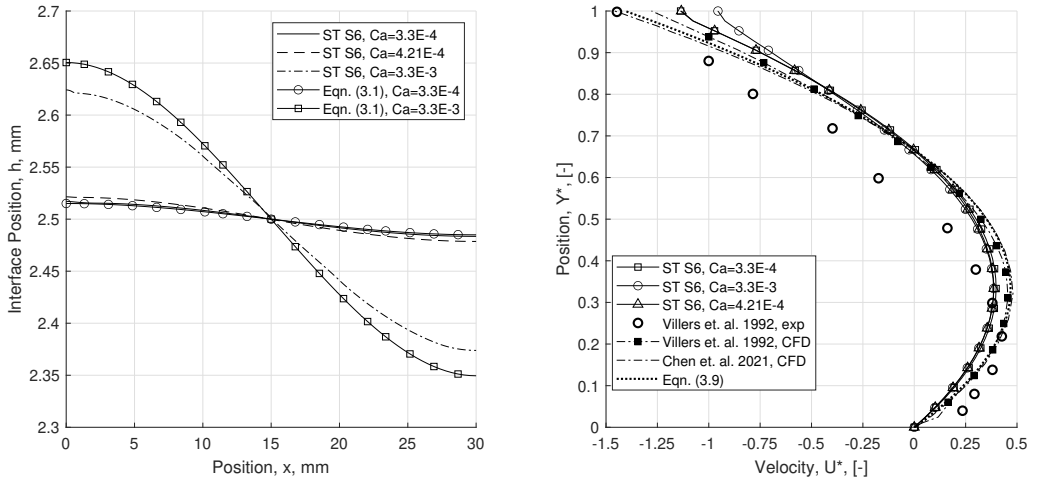

FIGURE 7. Effect of Capillary Number on interface position (left), and velocity profile at $x^* = L/2$ (right) in S6, constant Marangoni number 633, predictions from STAR-CCM+ (ST)

Marangoni number in the cases analysed. More generally, the true leading coefficient is likely a function of the nondimensional parameters, but based on the cases and ranges investigated it appears as a constant value. In figure 6, the velocity profile from all scenarios are plotted together with a constant Marangoni number. There is no obvious grouping and the peak velocity differs slightly between each scenario. Likely there is some other leading factor on (3.9) for each scenario.

5.2.1. *Effect of Capillary Number*

The model from Sen & Davis (1982) is most applicable to S6 and indeed the theory matches the effect of capillary number on the interface shape well in figure 7. Capillary number of $4.21E$-4 is based on the material properties of acetone and corresponds to the experiments from Villers & Platten (1992), although they did not measure the interface height in their work. The numerical results are mostly within the confidence range from

(3.1) of ± 17.4 μm. Disagreement with the theory can be attributed to the effects of the vapour phase which is not considered in the theoretical expression. In figure 7, the Capillary number is shown to not have much effect on the velocity profile. Disagreement from (3.9) is again attributed to the neglection of effects from the vapour phase. CFD results from Chen & Xu (2021) and Villers & Platten (1992) also show some disagreement as the previous work modelled the problem with a fixed flat interface and applied the surface tension forces along the wall boundary.

5.2.2. *Effect of Liquid Density*

The scenarios S1B and S3B had varying liquid density according to (2.26). In figure 5, S1B has a maximum interface height of nearly 1 (less than S1), with a slight positive slope, in this case smearing was present along the entire interface. The effect of variable liquid density in S1 is unclear due to the limitations of VOF method. S3B shows a larger maximum height compared to S3, presumably from liquid expansion near the hot end. Although scenarios S1, S3, S1B, and S3B have different maximum interface heights, each has nearly the same velocity profile as in figure 6. Therefore, (3.9) could be used to predict the velocity profile in a closed domain with or without buoyancy as in S1 or S3.

6. Conclusion

Due to the additional liquid convection and interface deformations from Marangoni forces, the effects of such should be considered in designing and analysing heat pipes. These flow-in-a-box cases show that significant fluid motion can occur from Marangoni forces alone. Depending on the material properties and flow conditions, Marangoni convection could enhance or deficit the overall heat transfer performance in such a device. For example, scenarios with a closed domain (S1,S3,S1B, and S3B) are the closest analogy to a conventional heat pipe. These cases all had a positive interface orientation, meaning in a heat pipe application, liquid would flood the hot end reducing possible dry out. If $\gamma > 0$, the liquid may starve the hot end, giving a performance deficit.

The velocity scale used with the analytical solutions from Sen & Davis (1982) is found to predict the profile and magnitude of the velocity in the liquid pool for S1 and S3 independent of the Marangoni number. The interface deformation from their expression predicts the effect of the Capillary number and is in agreement with S6.

The interface orientation was found to change sign and magnitude under various scenarios. Gravity was seen to have a negligible effect on velocity profiles and interface shape unless the domain was open, where the maximum interface height was much larger. Open domain scenarios had negative interface orientation, while closed domain scenarios had a positive orientation. Variable liquid density increased the maximum interface height observed, although the velocity profiles did not change significantly.

In almost all cases interface smearing was seen, but mass was still conserved to a high degree. Results are consistent between STAR-CCM+, openFOAM, previous CFD, and the theoretical expressions from Sen & Davis (1982).

Future work should investigate a larger range of Marangoni number, the effect of the domain aspect ratio, and differences in Prandtl number (motivated by the study from Zhou & Huang (2010)). The authors intend to further develop this model to include evaporation and condensation, and the effects of species concentration gradients. If these additional physics cannot be sufficiently combined with the present VOF model, then development will pivot to implementation of free surface Marangoni convection with other multiphase CFD approaches.

REFERENCES

Brackbill, J.U, Kothe, D.B & Zemach, C 1992 A continuum method for modeling surface tension. *Journal of Computational Physics* **100** (2), 335–354.

Chen, Enhui & Xu, Feng 2021 Transient marangoni convection induced by an isothermal sidewall of a rectangular liquid pool. *J. Fluid Mech.* **928**.

Nguyen, Thao T.T., Yu, Jiaheng, Wayner, Peter C., Plawsky, Joel L., Kundan, Akshay, Chao, David F. & Sicker, Ronald J. 2020 Rip currents: A spontaneous heat transfer enhancement mechanism in a wickless heat pipe. *International Journal of Heat and Mass Transfer* **149**, 119170.

Scheufler, Henning & Roenby, Johan 2021 Twophaseflow: An openfoam based framework for development of two phase flow solvers , arXiv: 2103.00870.

Sen, Asok & Davis, Stephen 1982 Steady thermocapillary flows in two-dimensional slots. *J. Fluid Mech.* **121**.

Smith, M.K. & Davis, S.H. 1983 Instabilities of dynamic thermocapillary liquid layer. *J. Fluid Mech.* **132**, 119–143.

Srimuang, W. & Amatachaya, P. 2012 A review of the applications of heat pipe heat exchangers for heat recovery. *Renewable and Sustainable Energy Reviews* **16** (6), 4303–4315.

Villers, Didier & Platten, Jean 1987 Separation of marangoni convection from gravitational convection in earth experiments. *PhysicoChemical Hydrodynamics* **8**, 173–183.

Villers, Didier & Platten, Jean 1992 Coupled buoyancy and marangoni convection in acetone: Experiments and comparison with numerical simulations. *J. Fluid Mech.* **234**, 487 – 510.

Zhou, Xiaoming & Huang, Hulin 2010 Numerical simulation of steady thermocapillary convection in a two-layer system using level set method. *Microgravity Science and Technology* **22**, 223–232.